



Deposited via The University of Leeds.

White Rose Research Online URL for this paper:

<https://eprints.whiterose.ac.uk/id/eprint/241004/>

Version: Supplemental Material

Article:

Vacca, A.V., Perez, J., Bellomo, K. et al. (2026) Subseasonal variability of the winter North Atlantic jet stream has decreased due to climate change. *Communications Earth & Environment*, 7. 382. ISSN: 2662-4435

<https://doi.org/10.1038/s43247-026-03423-0>

Reuse

Items deposited in White Rose Research Online are protected by copyright, with all rights reserved unless indicated otherwise. They may be downloaded and/or printed for private study, or other acts as permitted by national copyright laws. The publisher or other rights holders may allow further reproduction and re-use of the full text version. This is indicated by the licence information on the White Rose Research Online record for the item.

Takedown

If you consider content in White Rose Research Online to be in breach of UK law, please notify us by emailing eprints@whiterose.ac.uk including the URL of the record and the reason for the withdrawal request.

Supplementary Information

Subseasonal variability of the winter North Atlantic jet stream has decreased due to climate change

Authors:

Andrea Vito Vacca^{1,2}, Jacob Perez³, Katinka Bellomo⁴, Júlia Casadevall Díaz⁵, Ieuan Davies⁵, Jost von Hardenberg^{1,6}, Amanda Maycock⁵

Affiliations:

¹ Department of Environment, Land and Infrastructure Engineering, Polytechnic University of Turin, Turin, Italy.

² Istituto Universitario di Studi Superiori, Pavia, Italy

³ Centre for Doctoral Training in Fluid Dynamics, University of Leeds, Leeds, UK

⁴ Department of geoscience, University of Padua, Padova, Italy

⁵ School of Earth and Environment, University of Leeds, Leeds, UK

⁶ Istituto di Scienze dell'Atmosfera e del Clima, Consiglio Nazionale delle Ricerche (CNR-ISAC)

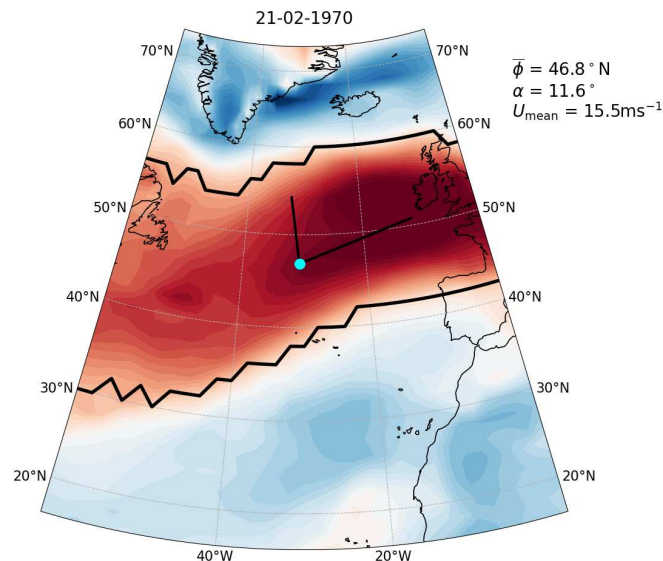


Figure S1: Daily zonal wind field (U_{a850}) for an example day in winter 1970/1971. The field is low-pass filtered with a Lanczos filter (61-day window, 10-day cut-off frequency). Solid contours denote the Eddy-driven Jet Object (EDJO) identified by the algorithm (see Methods). Light-blue dots denote the centre of mass of the EDJO with the

longer black line defining the major axis and the shorter the minor axis. The daily jet latitude (ϕ), tilt (α), and speed (U_{mean}) are indicated at the top right of the figure.

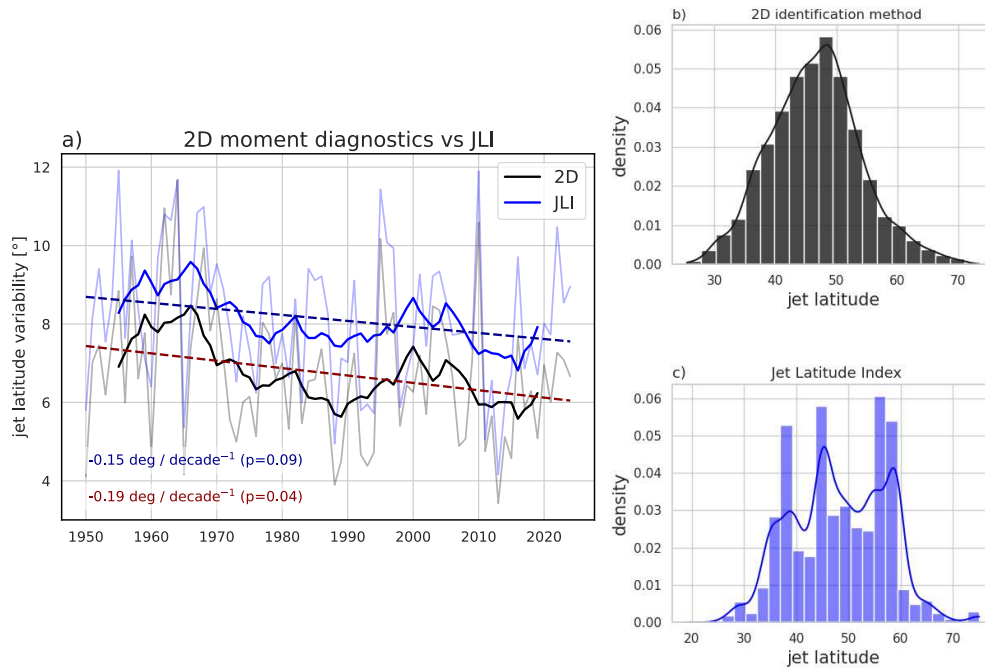


Figure S2: Comparison between 2D jet identification method and Jet latitude index. a) As Figure 1 but with the addition of the timeseries of jet latitude variability computed with the Jet Latitude Index method (JLI). b-c) distributions of winter daily jet latitudes in the two methods.

Supplementary Note 1: winter average trends in the jet

While the focus of the main text is on the jet subseasonal timescale variability, our methodology confirms the strengthening of the winter average North Atlantic jet ($0.08 \text{ ms}^{-1}\text{decade}^{-1}$). Additionally, we report a positive trend in the winter average jet tilt over 1950-2024 ($0.42^\circ\text{decade}^{-1}$), while the winter average jet latitude has remained unchanged (Figure S3 below).

Future climate change simulations disagree about trends in the winter average North Atlantic jet (Figure S9 below). Three of eleven models show an increase in seasonal mean jet latitude, four show a decrease and four show zero or marginal changes in jet latitude. The projected changes in seasonal mean jet speed and NAO index are also inconsistent across the models. However, there is greater model agreement in the simulated increase in winter average jet tilt (except for CanESM5).

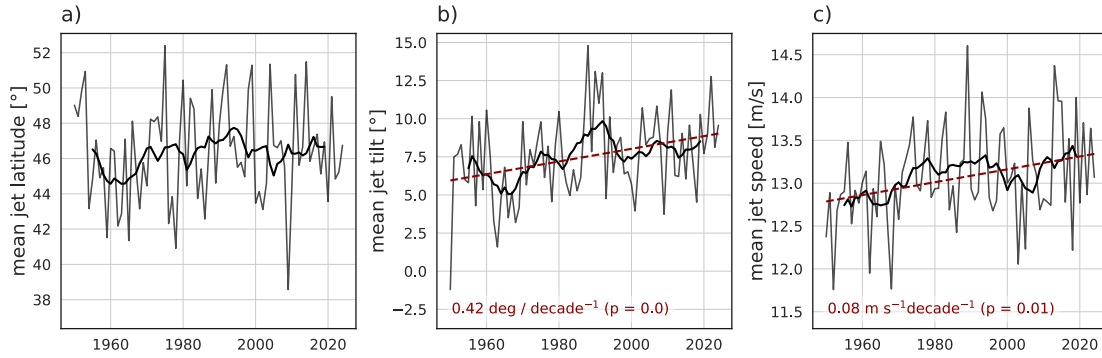


Figure S3: Time evolution of winter average North Atlantic eddy-driven jet. Timeseries (1950-2024) of North Atlantic eddy-driven jet winter average (a) latitude, (b) tilt and (c) speed in the ERA5 reanalysis dataset. Thick black lines represent the 11-year running mean. Red lines in (a) and (b) represent linear trends.

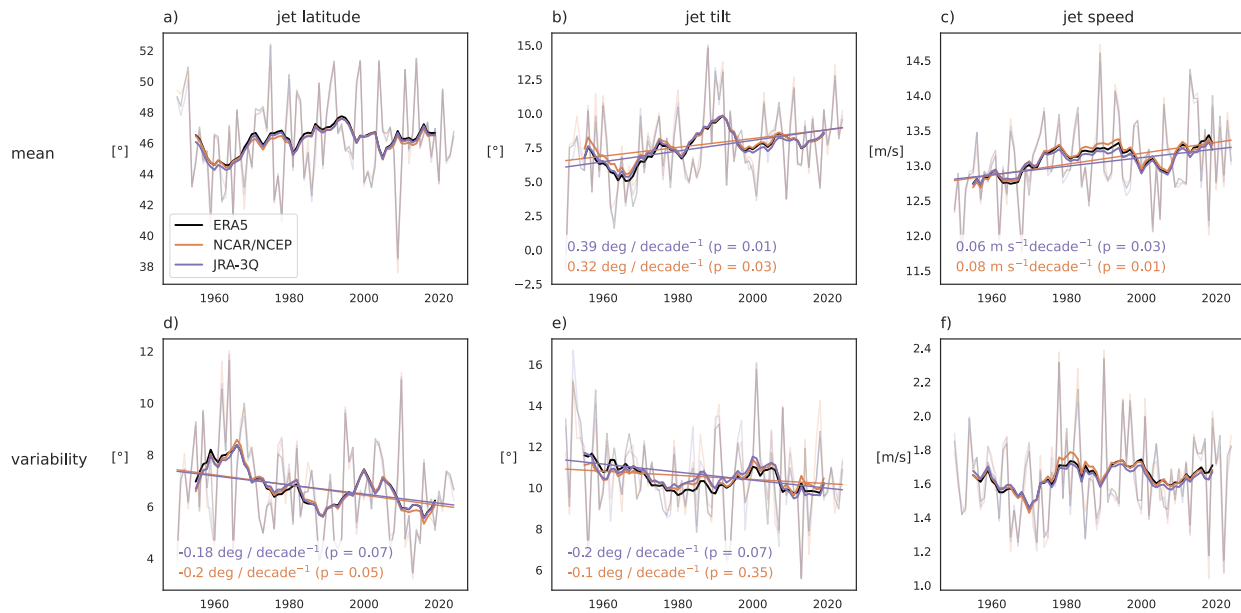


Figure S4: Comparison between different reanalysis products. Timeseries (1950-2024) of winter average (a) latitude, (b) tilt and (c) speed, and winter variability of (d) latitude, (e) tilt and (f) speed in ERA5, NCAR/NCEP and JRA-3Q reanalysis datasets. Thick lines represent the 11-years running means. Colored straight lines represent linear trends.

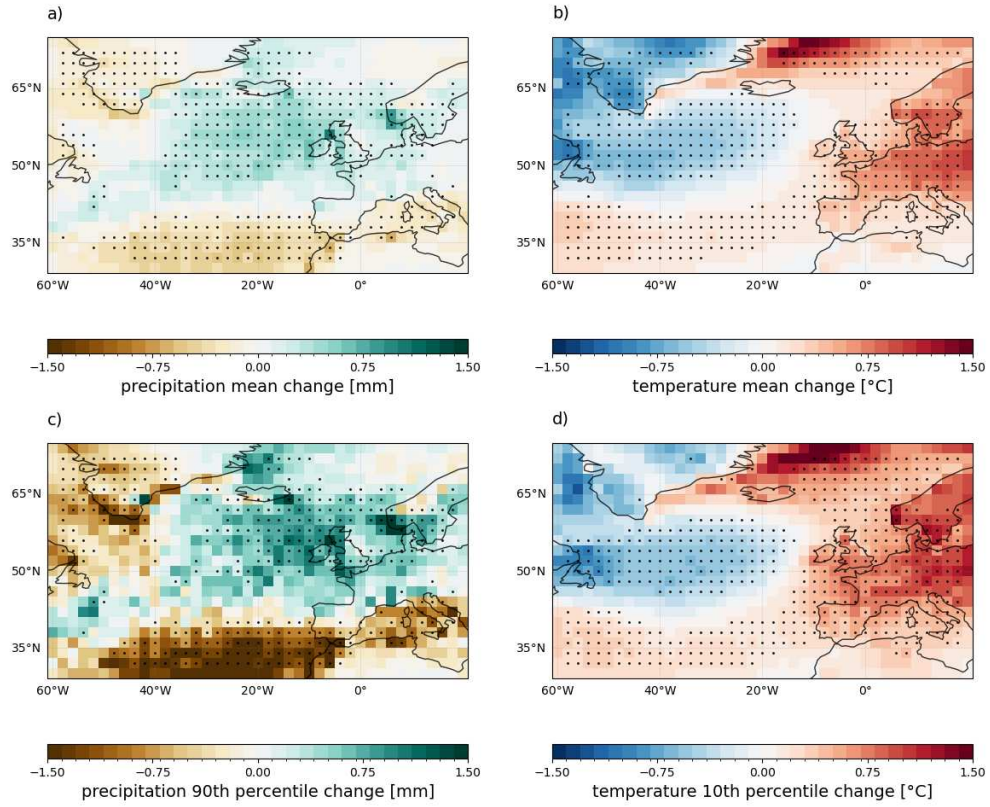


Figure S5: Additional climatic impacts of the decrease in North Atlantic eddy-driven jet latitude variability. As in Figure 2 but for (a) precipitation seasonal mean, (b) temperature seasonal mean, (c) precipitation 90th percentile, (d) temperature 10th percentile.

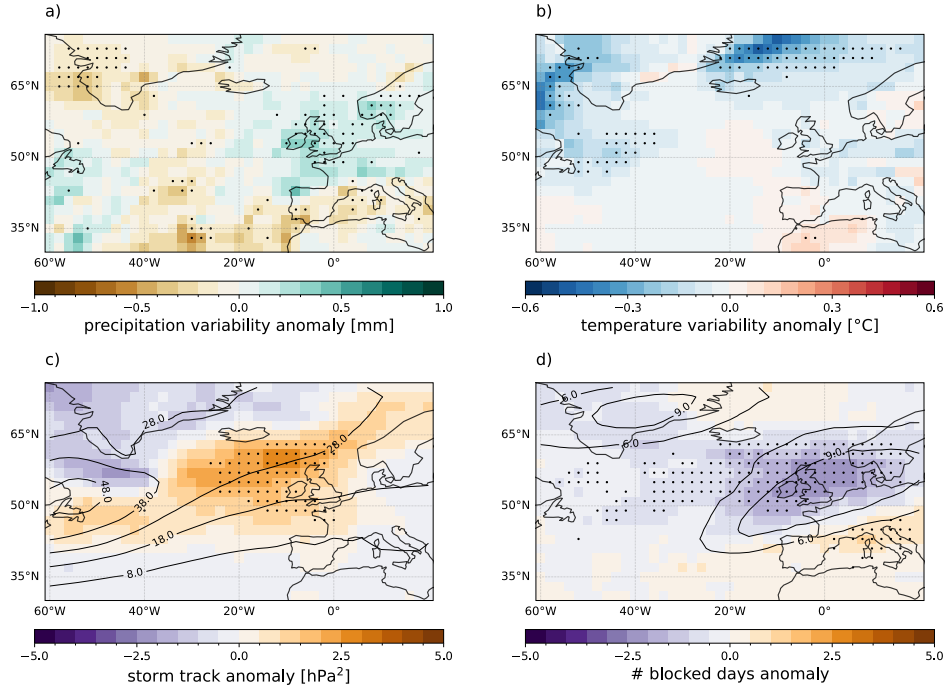


Figure S6: Climatic impacts of the decrease in North Atlantic eddy-driven jet tilt variability. As in Figure 2 but for tilt variability instead of latitude variability.

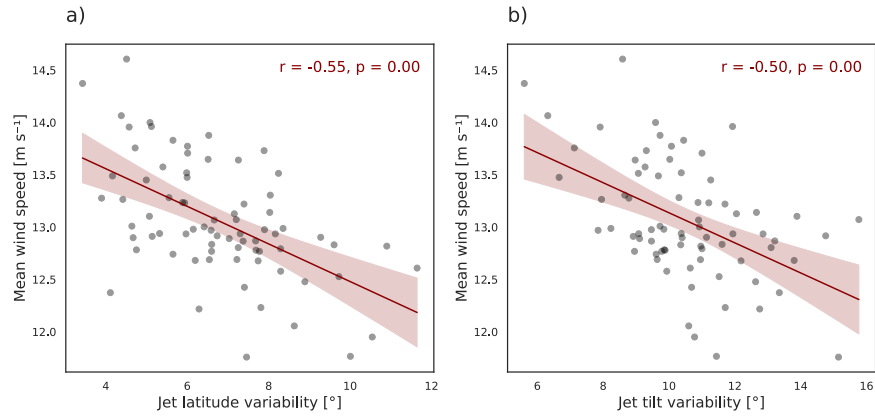


Figure S7: Relation between changes in the jet mean speed and variability in ERA5. Scatterplot of ERA5 North Atlantic eddy-driven jet winter variability of (a) latitude and (b) tilt vs the winter mean jet speed (1950-2024). The red line represents the interannual regression line.

Supplementary Note 2: correction of climate models low-frequency variance

We apply a linear scaling method to adjust the low-frequency variance of the climate model time series to that of ERA5. First, the low-frequency component X_L is extracted via a Butterworth filter with a 21-year cutoff frequency. The high-frequency residual is given by:

$$X_h = X - X_L$$

To match the observed variance of the low-frequency component, the scaling factor k is computed as:

$$k = \frac{std(X_L^{OBS})}{std(X_L)}$$

The rescaled low-frequency component is then defined as:

$$\widetilde{X}_L = (X_L - \overline{X}_L) * k + \overline{X}_L$$

Where the overbar indicates the time-average. Finally, the corrected time series is reconstructed by adding back the high-frequency residual:

$$\tilde{X} = \widetilde{X}_L + X_h$$

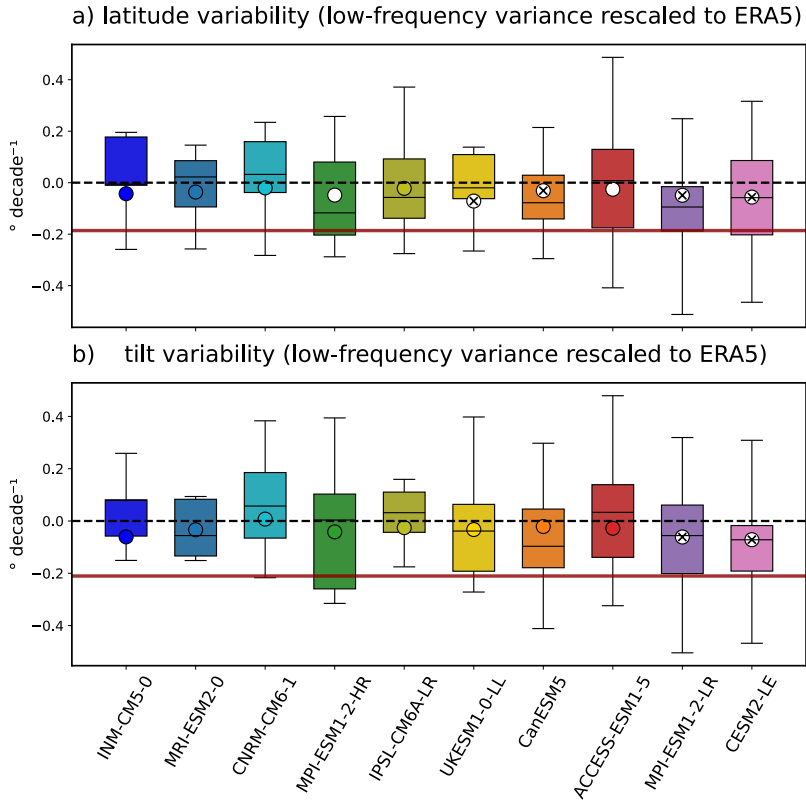


Figure S8: Comparison between rescaled climate models trends and ERA5 trends. As in Figure 3 but with climate models' low-frequency variance rescaled to match ERA5 (see Supplementary Note 2).

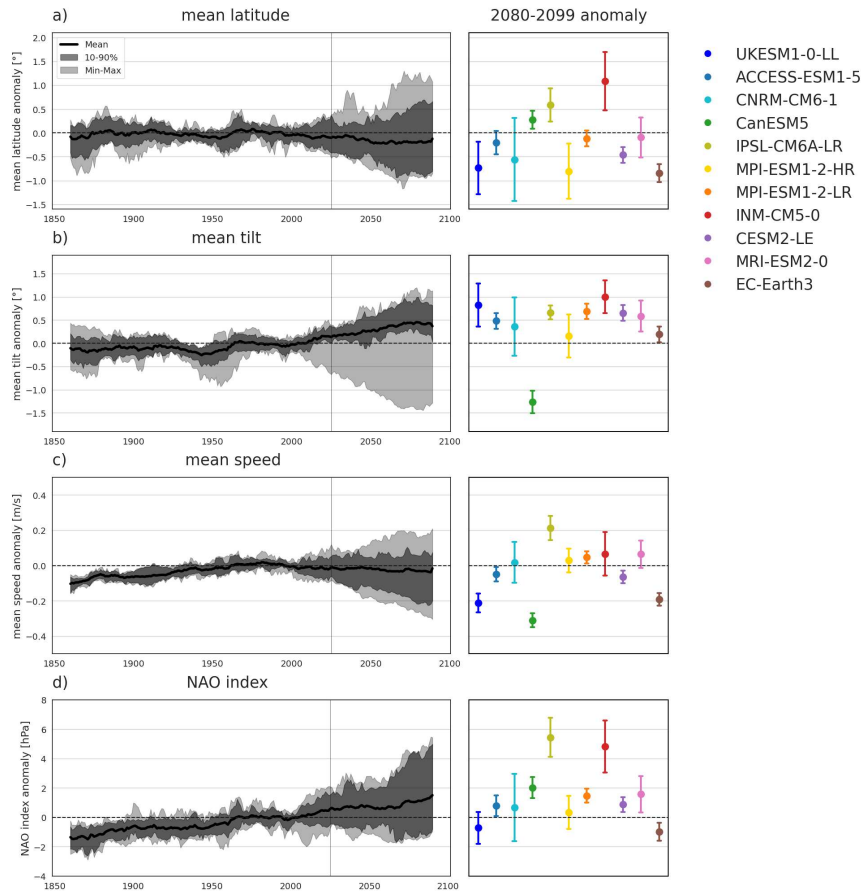


Figure S9: Projected evolution of the seasonal average jet diagnostics. As in Figure 4 but for of jet winter average (a) latitude, (b) tilt, (c) speed and (d) NAO index, The NAO index is computed as the difference in mean sea-level pressure between two boxes located on the Azores (28–20°W, 36–40°N) and Iceland (25–16°W, 63–70°N).

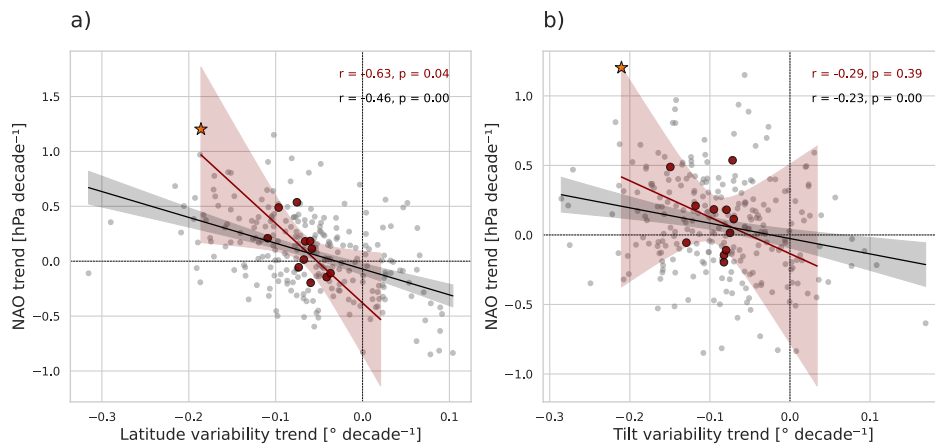


Figure S10: Relation between changes in the NAO index and changes in the jet variability. As in Figure 5 but with NAO index on the y-axis of mean jet speed. The NAO index is computed as the difference in mean sea-level pressure between two boxes located on the Azores (28–20°W, 36–40°N) and Iceland (25–16°W, 63–70°N).

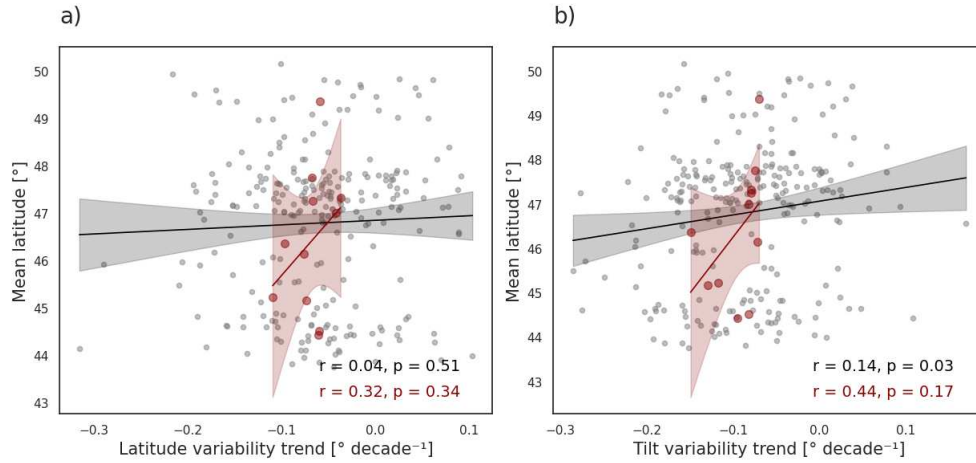


Figure S11: Relation between the climatological jet latitude and jet variability trends. Scatterplot of projected (2015-2100) linear trends in North Atlantic eddy-driven jet latitude (a) and tilt (b) variability vs. the mean (1970-2014) jet latitude. Unfilled dots represent data values in individual realisations with a linear regression in black, while filled dots show ensemble mean values for each model with the inter-model regression line in red. Light shading denotes the 95% uncertainty range on the regression lines.

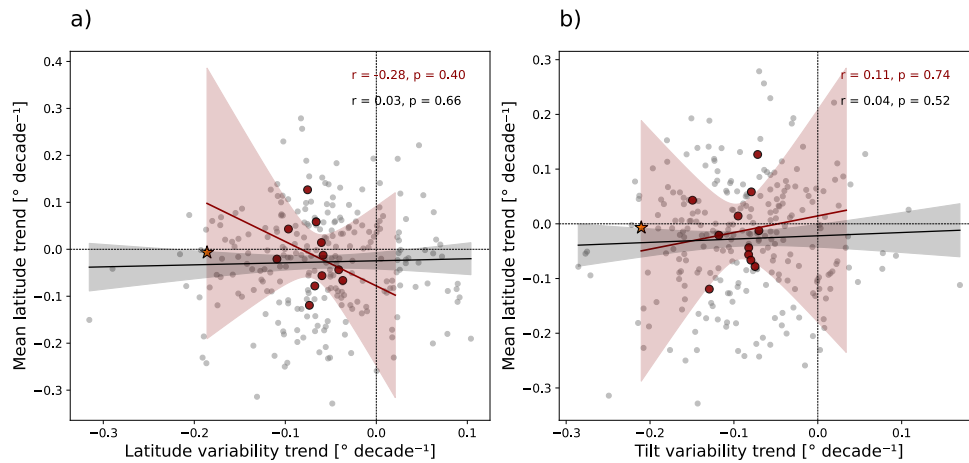


Figure S12: Relation between changes in the mean jet latitude and changes in the jet variability. As Figure 5 but with mean jet latitude on the y-axis.

Table S1: Latitude variability projected reduction for each model. Ensemble mean linear trends (2024-2099); value of the ensemble mean linear regressions in 2024 and 2099; Percent changes in 2099 relative to the 2024 value; Percent changes in 2099 relative to the ERA5 linear regression in 2024 (= 6.06°).

Model	Trend 2024-2099 [° decade ⁻¹]	2024 value [°]	2099 value [°]	Percent change [%]	Percent change vs ERA5 [%]
INM-CM5-0	-0.105	6.82	6.03	-11.58	-13
MRI-ESM2-0	-0.073	6.08	5.53	-9.05	-9.04
CNRM-CM6-1	-0.094	6.31	5.6	-11.25	-11.64
MPI-ESM1-2-HR	-0.089	6.24	5.57	-10.74	-11.02
IPSL-CM6A-LR	-0.108	5.67	4.85	-14.46	-13.37
UKESM1-0-LL	-0.078	6.6	6.01	-8.94	-9.66
CanESM5	-0.075	4.67	4.11	-11.99	-9.28
ACCESS-ESM1-5	-0.056	5.23	4.81	-8.03	-6.93
MPI-ESM1-2-LR	-0.05	5.64	5.27	-6.56	-6.19
CESM2-LE	-0.057	5.34	4.92	-7.87	-7.06
EC-Earth3	-0.054	5.95	5.55	-6.72	-6.68

Table S2: Tilt variability projected reduction for each model. Ensemble mean linear trends (2024-2099); value of the ensemble mean linear regressions in 2024 and 2099; Percent changes in 2099 relative to the 2024 value; Percent changes in 2099 relative to the ERA5 linear regression in 2024 (= 9.73°).

Model	Trend 2024-2099 [° decade ⁻¹]	2024 value [°]	2099 value [°]	Percent change [%]	Percent change vs ERA5 [%]
INM-CM5-0	-0.105	10.28	9.5	-7.59	-8.1
MRI-ESM2-0	-0.074	9.2	8.64	-6.09	-5.71
CNRM-CM6-1	-0.111	9.99	9.16	-8.31	-8.56
MPI-ESM1-2-HR	-0.15	9.73	8.61	-11.51	-11.57
IPSL-CM6A-LR	-0.166	9.02	7.78	-13.75	-12.8
UKESM1-0-LL	-0.089	9.24	8.58	-7.14	-6.86
CanESM5	-0.066	7.58	7.09	-6.46	-5.09
ACCESS-ESM1-5	-0.077	8.62	8.04	-6.73	-5.94
MPI-ESM1-2-LR	-0.089	9.13	8.46	-7.34	-6.86
CESM2-LE	-0.088	8.68	8.01	-7.72	-6.79
EC-Earth3	-0.09	9.32	8.64	-7.3	-6.94